Nanoscale

PAPER

View Article Online
View Journal | View Issue

Check for updates

Cite this: *Nanoscale*, 2018, **10**, 17807

Plasmonic targeting of cancer cells in a three-dimensional natural hydrogel†

Limor Minai, Matan Hamra and Dvir Yelin*

Received 25th April 2018,
Accepted 24th August 2018

DOI: 10.1039/c8nr03391a

rsc.li/nanoscale

Using specifically designed gold nanoparticles and local laser irradiation, individual cells and small cell clusters could be targeted on a microscopic scale with minimal toxicity to nearby tissue. To date, most scientific studies and technological demonstrations of this approach were conducted on two-dimensional cultures, while most feasibility tests and preclinical trials were conducted using animal models. For bridging the gap between two-dimensional cell cultures and animal experiments, we propose and demonstrate the use of a natural hydrogel for studying the effect of intense, ultrashort laser pulses on a gold nanoparticle targeted tissue. Using illumination parameters comparable to those used with two-dimensional cultures, we show the complete eradication of multilayered cell colonies comprising normal fibroblasts and malignant epithelial cells co-cultured on a hydrogel scaffold. By evaluating the extent of cell damage for various pulse durations at off-resonance irradiation, we find that the observed damage mechanism was dominated by rapid thermal transitions around the gold nanospheres, rather than by photoionization. The work provides a new tool for understanding the complex pulse–particle–tissue interactions and demonstrates the important role of nanoparticle mediated cavitation bubbles in a thick, multilayered tissue.

1. Introduction

Plasmonic cell manipulations mediated by the interaction between laser irradiation and gold nanoparticles have been shown to be promising for the selective targeting of cancer,[1,2] offering highly localized light–particle interactions, low residual cytotoxicity, and a wide range of potential cell damage mechanisms. Numerous research groups have studied and demonstrated plasmonic cell targeting by employing a variety of nanoparticles of different shapes (spheres,[2,3] rods,[4–6] shells[1,7] and others[8]) and irradiation parameters (continuous wave[2,5,8] and short pulses[4–6]), as well as in concert with chemotherapy[9] and immune system activation.[10] While 2D cell cultures are ideal for studying the detailed intracellular response to the plasmonic treatment, they often fail to mimic the complexity of *in vivo* environments; cell cultures in 2D cannot emulate the typically well-defined polarity in living tissue, which is known to affect intracellular signaling,[11,12] cell morphology[13] and phenotype,[12,14] as well as cell response to environmental cues that trigger apoptosis,[15] proliferation and differentiation.[16,17] Furthermore, 2D cell cultures often lack a normal extra-cellular matrix (ECM) that is vital for cell adhesion and signaling,[18] are often subjected to non-physiological mechanical forces,[10] and do not exhibit physiological gradients of nutrients and gases.[19,20] Consequently, animal models are often favored over cell cultures for studying tissue response to new drugs and to multifactorial therapeutic approaches. Successfully damaging tissue *via* plasmonic interactions has been demonstrated on murine models using gold nanoshells[1,7] and gold nanoparticles in combination with anti-cancer drugs.[21–23] Unfortunately, while providing an effective *in vivo* platform for preclinical experiments, animal models too often fail to accurately represent human physiology and genetics,[24–26] and hence are unable to correctly predict the complex human response to treatments; cancer therapies that were demonstrated effective in animals have shown less than 8% success in clinical trials.[27,28]

The wide experimental gap between 2D cell cultures and human subjects could, in many cases, be bridged using 3D cell cultures, in which cells are embedded within cell-supporting environments including tissue-derived spheroids,[11] pluripotent organoids,[29] biological and/or synthetic tissue scaffolds,[30] hydrogels,[31] small chips[32] and 3D-printed structures.[33] Compared to 2D cell cultures, 3D cultures would be more effective for studying laser therapy approaches, offering environments that more realistically mimic tissue optical parameters and more closely represent physiological conditions for studying, for example, the local delivery of treatment-mediating agents. Recently, a semi-synthetic 3D scaffold (polyethyl-

Faculty of Biomedical Engineering, Technion – Israel Institute of Technology, Haifa 3200003, Israel. E-mail: yelin@bm.technion.ac.il

†Electronic supplementary information (ESI) available. See DOI: 10.1039/c8nr03391a

ene glycol–heparin) has been demonstrated to be useful for providing an *in vitro* environment suitable for studying laser pulse targeting of glioblastoma cells conjugated by gold nanorods.[34] Gold nano-stars and continuous-wave illumination were used to study the eradication of small breast cancer tumor emboli in suspension.[35]

In this work, we study the plasmonic targeting of malignant epithelial breast cancer cells co-cultured with normal foreskin fibroblasts, all embedded and cultured in a three-dimensional natural hydrogel. Following the attachment of gold nanospheres coated by anti-EGFR antibodies to the cells, the cultures were irradiated by a sequence of high-intensity off-resonance pulses and continuously monitored using time-lapse microscopy for studying the culture response over the course of several days. We show that the total pulse energies required for the effective elimination of the cell colonies were comparable to 2D cultures,[36,37] despite the notable differences in cell arrangement, irradiation wavelength, and the underlying cell damage mechanisms, dominated here by disruptive thermally driven processes and not by multiphoton ionization.[38]

2. Results

Epithelial breast cancer MDA-MB-468 cells seeded on the top surface of a 4% Matrigel hydrogel formed unicellular networks after approximately 1.5 hours (Fig. 1a). Over time, the networks developed into cell colonies interconnected by thin unicellular extensions that were later retracted, leaving isolated dense multilayered colonies on the gel. Eight hours after seeding, the cultures were incubated for 16 hours with 20 nm-diameter gold nanospheres conjugated to anti-EGFR molecules with high affinity to the EGFR overexpressed on the cancer cell membranes. The presence of nanoparticles within the cell culture was verified using two-photon excitation fluorescence microscopy (Fig. 1b), showing particle attachment deep within the colonies. Twenty-four hours after seeding, the cells were irradiated by scanning a high irradiance (0.3 TW cm^{-2}, 1 kHz) 45 fs pulse laser beam at an off-resonance 800 nm center wavelength, resulting in up to 20 pulses irradiating each location on the gel. Time lapse imaging (Fig. 2a) of the irradiated cultures was conducted at the rate of one frame every 5 minutes for the first 10 hours, followed by one frame every hour over several days. The culture medium was replaced every 24 hours to prevent dehydration and provide fresh nutrients. Whereas in the absence of nanoparticles the irradiated cell population gradually grew into large, multi-layered opaque cell colonies (Fig. 2a, top row and the ESI Movie 1†), the irradiated cultures with nanoparticles slowly disintegrated several hours after irradiation, until no living cells remained within the field of view 400 hours after irradiation (bottom row in Fig. 2a and the ESI Movie 2†). Colony disintegration was strongly dependent on the number of irradiating pulses – six pulses slightly reduced colony growth while twelve pulses strongly inhibited colony growth but did not eliminate all the cells, allowing the remaining cells to grow back into small colonies after

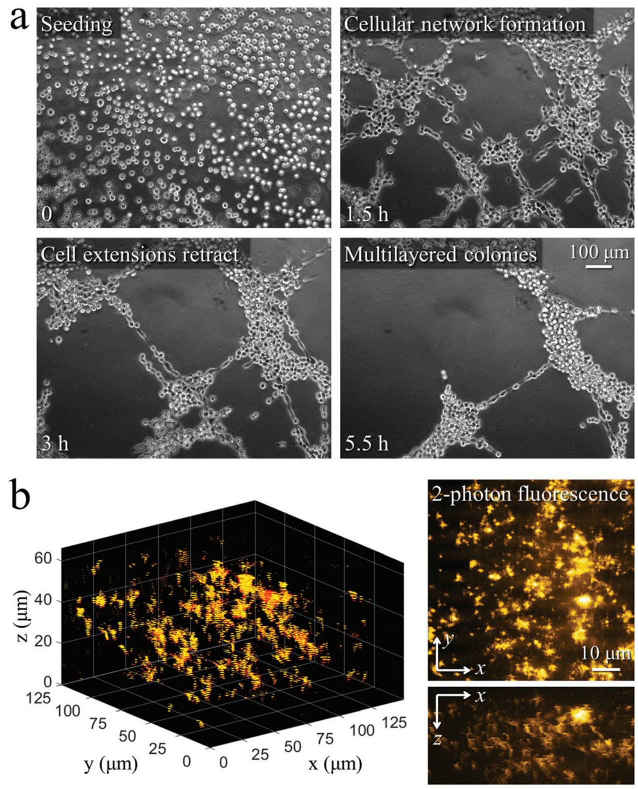

Fig. 1 Cell colony formation and nanoparticle targeting. a. Time-lapse widefield microscopy of MDA-MB-468 cell growth from seeding to the formation of multilayered colonies. b. Two-photon excitation fluorescence microscopy analysis of a colony targeted by anti-EGFR-coated 20 nm-diameter gold nanospheres revealed the 3D distribution of the nanospheres (yellow) deep within the cell colony.

150 hours. Colony size estimation was done using a specialized software code (Matlab) that integrated all pixel values in the colony image for calculating the total optical opacity of the cell cultures in visible light (Fig. 2b); colony growth rapidly decreased with the increasing number of pulses, from an 8.6-times increase in opacity level for the control particle-free colonies, down to a 250-times opacity reduction in the nanoparticle-targeted culture, 400 hours after irradiation.

Under similar irradiation conditions (20 pulses, 800 nm wavelength, 0.3 TW cm^{-2}) 2D cultures of MDA-MB-468 cells have shown similar trends of cell damage and elimination. As shown in the ESI Fig. 1,† the 2D cultures exhibited significant (80%) drop in the number of live cells 50 hours after irradiation, while the irradiated particle-free cultures continued to grow by more than 50% during 50 hours.

In order to study the potential of plasmonic therapy for targeting malignant cells in the context of a connective tissue comprising normal stromal cells,[39] human foreskin fibroblasts (HFFs) were seeded on top of a 4% Matrigel, forming cellular networks that rapidly developed into isolated colonies comprising densely packed round cells (Fig. 3, 2–10 hours). Malignant MDA-MB-468 cells added (1 : 1 ratio) to the culture 24 hours after HFF seeding formed cellular networks that were

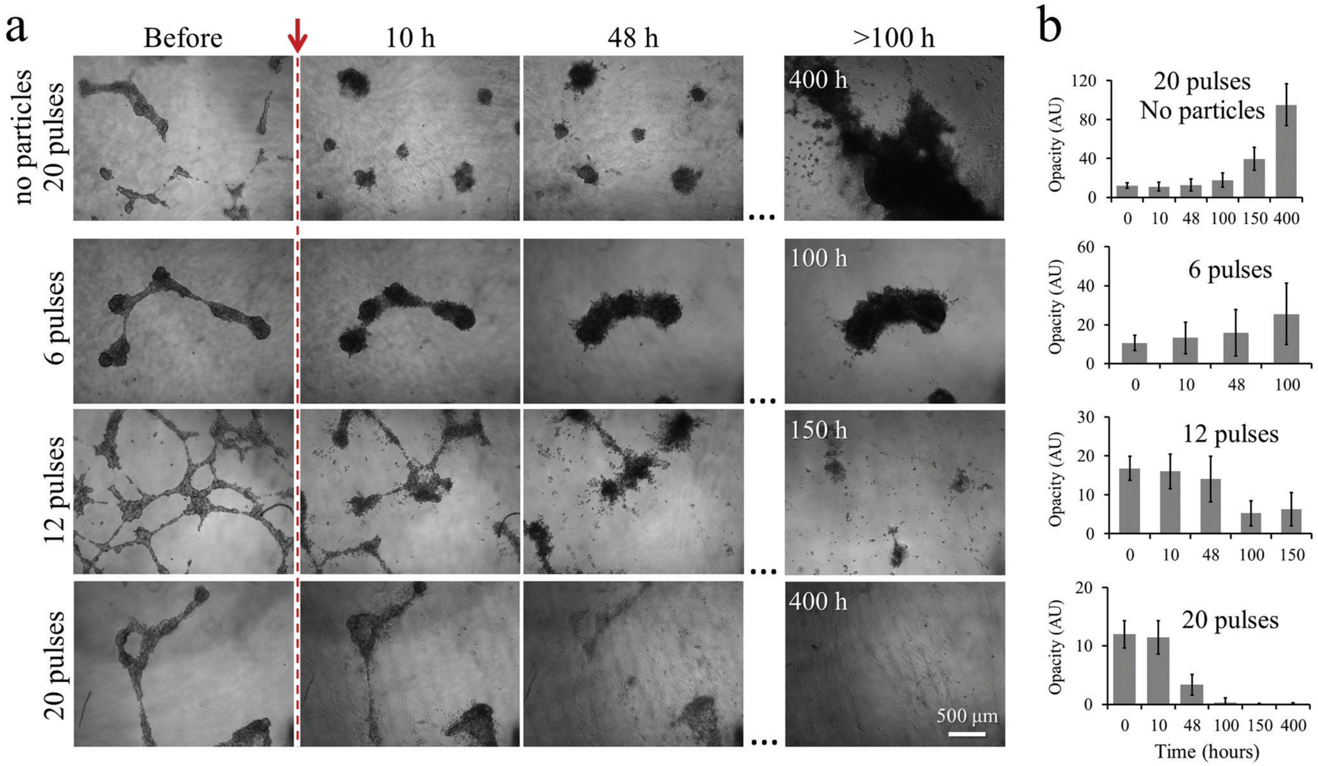

Fig. 2 Time-lapse microscopy image of plasmonic eradication of MDA-MB-468 cell colonies. a. Widefield images show inhibited growth of the dark cell colonies with increasing number of pulses. Complete colony destruction was observed 400 hours after irradiation by 20 pulses. Pulse duration was 45 fs, with 0.3 TW cm^{-2} peak power (13.5 mJ cm^{-2}) and 800 nm central wavelength. The red arrow and the dashed line indicate the time of irradiation. b. The measured optical opacity of the colonies at different times after irradiation. Error bars represent standard deviations.

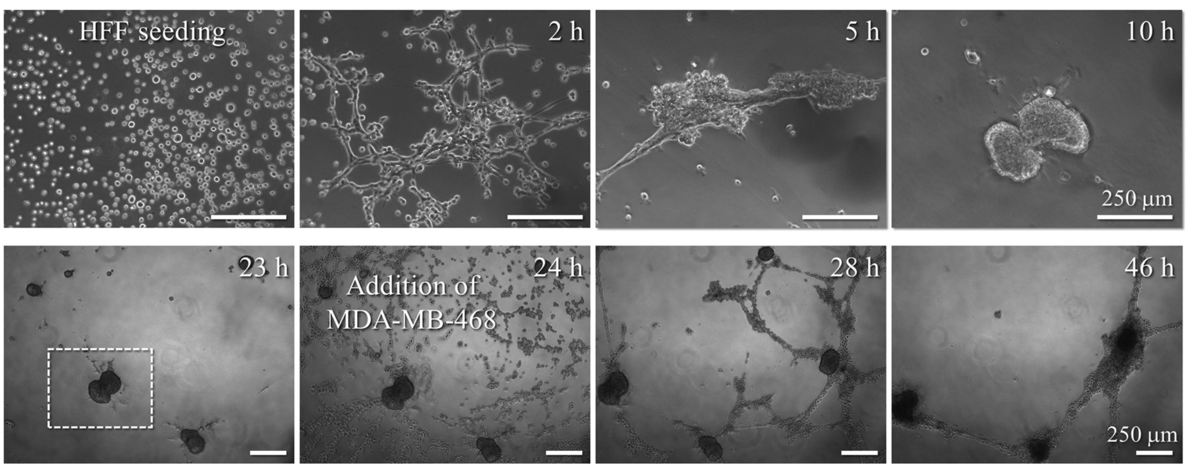

Fig. 3 Formation of cell colonies in HFF : MDA-MB-468 cell co-culture (1 : 1 ratio). 2–23 h: HFF cell growth into small multilayered colonies. 24 h: Addition of malignant MDA-MB-468 cells. 24–46 h: Gathering of the MDA-MB-468 cells around the HFF colonies. Scale bars represent 250 µm.

gradually wrapping around the existing HFF colonies (Fig. 3, 24–46 hours). Irradiation (30 pulses, 45 fs, 0.3 TW cm^{-2}) of the control co-cultures (without nanoparticles) had no effect on the cells that sustained their growth and developed into large colonies (Fig. 4a and the ESI Movie 3†). Laser irradiation of the nanoparticle-targeted co-culture resulted in a complete halt of colony growth (Fig. 4a and the ESI Movie 4†), followed by gradual colony disintegration between 5 and 48 hours after irradiation. Image analysis of the time lapse images revealed approximately 157% increase and a 7-times decrease in total cell opacity (400 h after irradiation) for the nanoparticle-free and the nanoparticle-targeted co-cultures, respectively (Fig. 4b). Eradication of cells in co-cultures with a higher malignant-to-normal cell ratio of 6 : 1 showed higher resilience

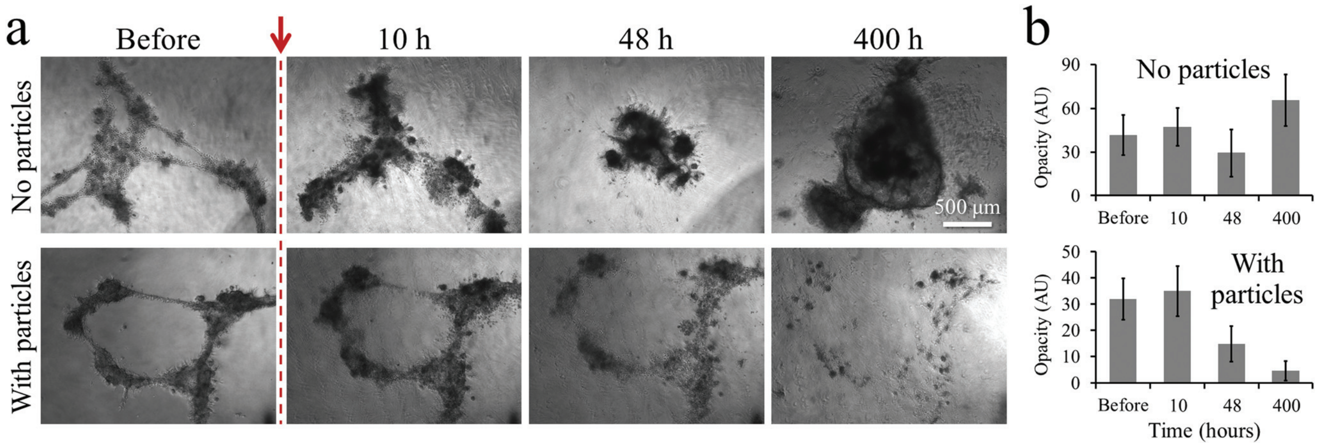

Fig. 4 Plasmonic eradication of HFF : MDA-MB-468 (1 : 1) co-cultures. a. Time lapse widefield microscopy of irradiated control and nanoparticle-targeted co-cultures. The red arrow and the dashed line indicate the time of irradiation. b. Colony optical opacity at different times following irradiation. The particle-targeted colony did not recover even 400 h after irradiation. Error bars represent standard deviations.

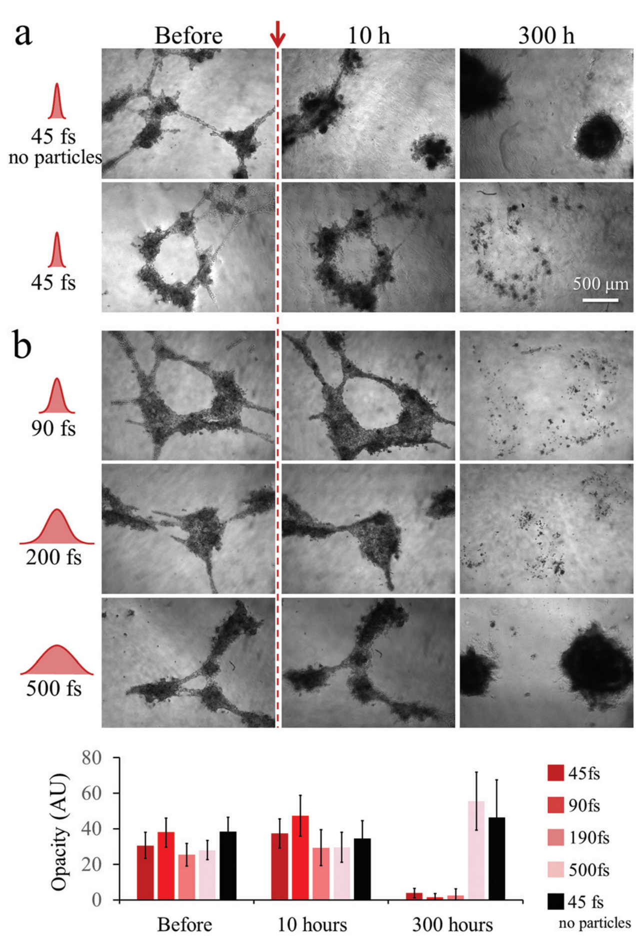

Fig. 5 Effect of pulse duration on colony damage. HFF : MDA-MB-468 co-cultures in a 1 : 6 cell ratio were heavily damaged using 45 fs, 90 fs and 200 fs, but appeared unaffected following 500 fs pulse irradiation. The red arrow and the dashed line indicate the time of irradiation. Error bars represent standard deviations.

of the colonies to the laser irradiation, requiring twice the number of pulses (60 pulses) for delivering substantial damage (Fig. 5a), whereas control, particle-free cultures continued to evolve after irradiation; irradiated colonies with nanoparticles ceased their growth and disintegrated less than 24 hours after irradiation.

The need for additional laser pulses for eradicating colonies with a higher malignant-to-normal cell ratio could suggest that the damage to the colonies was primarily energy-dependent, rather than peak-power dependent.[38] To reveal the dominant physical mechanism responsible for the observed cell damage, co-cultures with a similar (6 : 1) malignant-to-normal cell ratio were irradiated by pulse trains (60 pulses) of various pulse durations of 45 fs, 90 fs, 200 fs, and 500 fs (Fig. 5b); pulse energies had remained constant (0.18 mJ) during the experiment, resulting in substantially lower peak powers (4 GW, 2 GW, 0.9 GW and 0.36 GW, respectively) for the longer duration pulses. Up to 200 fs, the substantial extent of cell damage remained unaffected despite pulse broadening by a factor of 4.4. For the 500 fs pulses, however, no visible damage to the colonies was evident (Fig. 5b, the lowest panels), suggesting that the cell damage observed throughout this work was most likely dominated by rapid thermally driven effects (*i.e.* mechanical shock waves and cavitation bubbles) and not by multiphoton ionization, which is a strongly nonlinear peak-power dependent process.

3. Discussion

Compared with standard cell cultures on a glass substrate, 3D cultures can more closely imitate small solid tumors, and would thus be more suitable for preliminary studies of therapeutic approaches aiming to target various malignancies embedded within a healthy tissue. In particular, photothermal therapy techniques that rely on specific mediating agents could greatly benefit from such models that allow studying the underlying damage mechanisms, understand the various parameters affecting tumor eradication, and demonstrate the promises and limitations of each approach.

Our experiments with thick cell colonies grown on natural hydrogels have revealed various aspects related to laser–tissue interactions and pointed to some of the challenges associated with nanoparticle-mediated laser therapy in general. First, our initial experiments showed that thick MDA-MB-468 cell cultures exhibited comparable damage thresholds with those exhibited by equivalent 2D cultures; one should keep in mind, however, that numerous factors are often involved in colony damage, including non-specific particle attachment to the hydrogel and different cell morphology – rounded compact cells in 3D and strongly adhered to the flat glass substrate in 2D. This finding is somewhat different from previous results reported by Gonçalves *et al.*[34] and Crawford *et al.*[35] on less effective photothermal damage in 3D semi-synthetic hydrogels and in tumor emboli suspension. Second, co-cultures of malignant and normal fibroblast cells required higher irradiation doses (1.5 times the number of pulses compared to homogeneous cultures) for achieving complete disintegration of the cell colonies. The higher damage thresholds could be due to the support provided by the stromal cells (fibroblasts) to the colonies.[40–42] Thickening of the colonies also reduced light penetration into deep cell layers, hence requiring higher pulse energies for damaging the entire colony. Third, as shown in Fig. 4 and 5, eradication of the cell colonies included also the death of the normal fibroblasts, suggesting either particle binding to the hydrogel components in close proximity to the cells (see the ESI Fig. 2a† for nonspecific damage to irradiated HFF cells), or the involvement of collateral damage mechanisms that extend beyond the nanometric-scale environments around the particles. Fourth, the large clusters of gold nanospheres that are formed throughout the hydrogel may shift the resonance wavelength to the near infrared range; hence, the 800 nm wavelength used in our experiments may be more effective for targeting tissue regions with larger aggregates. Finally, our results with varying pulse durations (Fig. 5) indicate that the colony damage was mainly triggered by dominant cell-destructive photothermal processes[43–45] around the nanoparticles. Unlike in our previous work with 2D cultures, where multiphoton ionization dominated cell damage at on-resonance irradiation,[38] here the colony damage was found to be insensitive to changes in pulse duration up to a few hundreds of femtoseconds. The negligible cell damage at relatively long pulse durations of 500 fs (Fig. 5) indicates that the dominant damage mechanism was most likely thermally driven cavitation bubbles,[46,47] which require pulses that are shorter compared to the particles' heat diffusion time constants, resulting in a rapid heating of the nanoparticles to well above melting temperatures. Particle expansion and water evaporation around the particles then generated mechanical shock waves[45,48] that may inflict substantial mechanical damage to the nearby tissue. For shorter pulses, the resulting higher peak powers increased the multiphoton ionization efficiency within and around the gold nanoparticles; still, the weak dependence of colony damage on pulse duration between 45 fs and 200 fs suggests that multiphoton ionization is less harmful to the colonies compared with the dominant thermally driven damage.

4. Conclusion

In summary, eradication of thick cancer cell colonies grown on a natural hydrogel was demonstrated using a series of intense ultrashort pulses of durations between 45 and 200 fs. The three-dimensional cell colonies exhibited similar damage thresholds compared to 2D cultures, despite the numerous obvious differences in the experimental parameters. Co-culturing the cancer cells with normal fibroblasts improved the resistance of the colonies to laser light, most likely due to the improved cell viability within the co-cultures. The dominant thermally driven damage mechanism was also different from the photoionization damage that dominated our previous studies with resonantly irradiated 2D cell cultures, suggesting clear differences in cell environment and in the pulse–particle interactions between these experimental settings. The results of this work demonstrate the potential of 3D cell cultures for advancing the research of nanoparticle mediated cancer therapy using intense laser pulses. The physical environments provided by the hydrogels may offer a closer representation of small solid tumors compared to 2D cultures, allowing studying the complexity of the light–particle–tumor interactions under more realistic conditions.

5. Experimental data

Cell culture

MDA-MB-468 epithelial cells (American Type Culture Collection) and human foreskin fibroblast (HFF) cells were grown at 37 °C and 5% CO_2 in DMEM medium (Sigma). The medium was supplemented with 2 mM glutamine and 5 mM sodium pyruvate for the MDA-MB-468 cells and 0.1 mM β-mercaptoethanol and 0.1 mM MEM for the HFF cells in addition to 10% heat-inactivated fetal bovine serum. Cell cultures were seeded on top of Matrigel (Corning) hydrogel extracted from mouse sarcoma, containing growth factors and ECM proteins that are essential for cell growth and differentiation. The total protein concentration was 4 mg ml^{-1} with 200 μl Matrigel gel per 1 cm^2 well. Approximately 0.3×10^5–1.7×10^5 cells were seeded in each well.

Nanoparticle preparation

Gold nanoparticles were prepared using a citrate reduction protocol[49] resulting in an average particle diameter of 20 nm. Anti-EGFR (Lab Vision, clone designation EGFR.1) coating was carried out according to Weiss *et al.*[50] Shortly, anti-EGFR was incubated with OPSS-PEG2000-NHS (PEGWorks) for 1 h in a mole ratio of 1 : 2500, followed by an additional 1 h incubation with gold nanospheres in a mole ratio of $1:10^6$ nanospheres : OPSS-PEG2000-NHS.

Cell targeting by nanoparticles

MDA-MB-468 cells and/or human foreskin fibroblasts (0.3×10^5–1.7×10^5 cells) were grown on Matrigel hydrogel for 8 to 36 hours, followed by incubation for 16 hours at 37 °C with 1.5×10^{11} anti EGFR-coated gold nanoparticles. Cells were washed from unbound nanoparticles (three medium washes) prior to laser irradiation. By measuring the concentration of the washed-off particle solution, we estimate an average binding of approximately 3×10^5 nanoparticles per cell. Control experiments were conducted in parallel to all experimental procedures, including particle-targeted cells without irradiation and irradiation of cells without nanoparticles.

Two photon microscopy

A beam from a Ti:sapphire oscillator (25 fs, 80 MHz, 800 nm) was scanned using two galvanometric scanners (Cambridge Technology), magnified, and focused onto the sample using a 60×, NA = 1.2 water-immersion objective. The average power on the sample was approximately 90 mW. Two-photon excited fluorescence was filtered using a short-pass dichroic mirror (700 nm threshold wavelength, Chroma Technology) and a barrier filter (E680SP-2P, Chroma Technology), and measured using a photomultiplier tube (H7422-40, Hamamatsu Photonics). Prior to imaging, cells were fixed using 4% paraformaldehyde. *Z*-Projection images include the summation of 66 frames captured at 1 μm intervals along the *z*-axis. The exposure time was 12.5 μs per pixel.

Laser pulse irradiation

A beam from an amplified Ti:sapphire oscillator (Spitfire Pro XP and MaiTai, Newport Corp.) centered at 800 nm wavelength was coupled into one of the ports of an inverted microscope (Nikon Eclipse Ti). Pulse duration was adjusted between 45 fs and 500 fs by tuning the pulse compressor parameters inside the amplifier. Pulse durations below 100 fs were measured by interferometric autocorrelation (Femtometer™, Femtolasers Produktions GmbH), while longer pulse durations were measured by calculating the relative drop in the pulse intensity autocorrelation. Pulse intensity was controlled by adjusting the angle between a half-wave plate and a linear polarizer. Irradiated cells were first placed in eight-well chamber slides (Lab-Tek II, Thermo Scientific; 200 μl hydrogel per well) within a microscope stage incubator (Okolab Inc.) at controlled temperature and CO_2 concentration. A circular 400 μm-diameter Gaussian beam was used to irradiate a total area of 1 cm^2 using a matrix of 25 × 25 spots, where the lateral beam scan rate was adjusted to obtain the desired number of pulses illuminating each sample location. Beam profile was measured using a Spiricon laser beam sampler (LBS 100, Ophir). Experiments at each set of irradiation parameters were repeated at least three times.

Data analysis

Images of cells acquired immediately after irradiation and up to 400 h after irradiation were selected from a time-lapse series and used for the quantification of cell growth. Selected images from the time-lapse image series were analyzed using a dedicated Matlab code for estimating the size of the cell colonies. Each image was inverted and background subtracted, followed by the computation of a binary mask that corresponds to the effective area covered by the cells. The optical opacity at each pixel within the colony area was calculated as the difference between the pixel value and the background level from a nearby cell-free region. The total sample opacity reported in Fig. 2, 4, and 5, which is correlated with the total number of the cells, was calculated by integrating the overall opacity values at all pixels within the area of the colonies. The live cells in the ESI, Fig. 1† were manually counted.

Conflicts of interest

The authors declare no conflict of interest.

References

1 D. P. O'Neal, L. R. Hirsch, N. J. Halas, J. D. Payne and J. L. West, *Cancer Lett.*, 2004, **209**, 171–176.
2 I. H. El-Sayed, X. Huang and M. A. El-Sayed, *Cancer Lett.*, 2006, **239**, 129–135.
3 X. Huang, B. Kang, W. Qian, M. A. Mackey, P. C. Chen, A. K. Oyelere, I. H. El-Sayed and M. A. El-Sayed, *J. Biomed. Opt.*, 2010, **15**, 058002.
4 H. Takahashi, T. Niidome, A. Nariai, Y. Niidome and S. Yamada, *Chem. Lett.*, 2006, **35**, 500–501.
5 L. Tong, Y. Zhao, T. B. Huff, M. N. Hansen, A. Wei and J. X. Cheng, *Adv. Mater.*, 2007, **19**, 3136–3141.
6 J. L. Li, D. Day and M. Gu, *Adv. Mater.*, 2008, **20**, 3866–3871.
7 L. R. Hirsch, R. J. Stafford, J. A. Bankson, S. R. Sershen, B. Rivera, R. E. Price, J. D. Hazle, N. J. Halas and J. L. West, *Proc. Natl. Acad. Sci. U. S. A.*, 2003, **100**, 13549–13554.
8 H. Yuan, A. M. Fales and T. Vo-Dinh, *J. Am. Chem. Soc.*, 2012, **134**, 11358–11361.
9 R. Zhao, X. Han, Y. Li, H. Wang, T. Ji, Y. Zhao and G. Nie, *ACS Nano*, 2017, **11**, 8103–8113.
10 Z. Shaohui, N. Van Du, S. Seung Yoon, H. Jiwon and P. Jong-Oh, *Nanotechnology*, 2017, **28**, 435102–435116.
11 E. Cukierman, R. Pankov, D. R. Stevens and K. M. Yamada, *Science*, 2001, **294**, 1708–1712.
12 R. S. Gieni and M. J. Hendzel, *J. Cell. Biochem.*, 2008, **104**, 1964–1987.
13 M. Larsen, V. V. Artym, J. A. Green and K. M. Yamada, *Curr. Opin. Cell Biol.*, 2006, **18**, 463–471.
14 O. W. Petersen, L. Rønnov-Jessen, A. R. Howlett and M. J. Bissell, *Proc. Natl. Acad. Sci. U. S. A.*, 1992, **89**, 9064–9068.

15 V. M. Weaver, O. W. Petersen, F. Wang, C. A. Larabell, P. Briand, C. Damsky and M. J. Bissell, *J. Cell Biol.*, 1997, **137**, 231.
16 R. McBeath, D. M. Pirone, C. M. Nelson, K. Bhadriraju and C. S. Chen, *Dev. Cell*, 2004, **6**, 483–495.
17 C. S. Chen, *J. Cell Sci.*, 2008, **121**, 3285.
18 S. Zhang, X. Zhao and L. Spirio, *PuraMatrix: Self-assembling peptidenanofiber scaffolds*, CRC Press, Boca Raton, FL, 2005.
19 H. L. Ashe and J. Briscoe, *Development*, 2006, **133**, 385–394.
20 B. M. Baker and C. S. Chen, *J. Cell Sci.*, 2012, **125**, 3015.
21 J. Zhou, Z. Wang, Q. Li, F. Liu, Y. Du, H. Yuan, F. Hu, Y. Wei and J. You, *Nanoscale*, 2015, **7**, 5869–5883.
22 H. Wang, R. Zhao, Y. Li, H. Liu, F. Li, Y. Zhao and G. Nie, *Nanomedicine*, 2016, **12**, 439–448.
23 J. Liu, C. Abshire, C. Carry, A. B. Sholl, S. H. Mandava, A. Datta, M. Ranjan, C. Callaghan, D. V. Peralta, K. S. Williams, W. R. Lai, A. B. Abdel-Mageed, M. Tarr and B. R. Lee, *BJU Int.*, 2017, **119**, 342–348.
24 B. Davies and T. Morris, *Pharm. Res.*, 1993, **10**, 1093–1095.
25 J. C. L. Schuh, *Toxicol. Pathol.*, 2004, **32**, 53–66.
26 A. Gawrylewski, *Scientist*, 2007, **21**, 45.
27 N. Shanks, R. Greek and J. Greek, *Philos. Ethics Humanit. Med.*, 2009, **4**, 2–2.
28 I. W. Y. Mak, N. Evaniew and M. Ghert, *Am. J. Transl. Res.*, 2014, **6**, 114–118.
29 M. A. Lancaster and J. A. Knoblich, *Science*, 2014, **345**, 1247125.
30 E. Carletti, A. Motta and C. Migliaresi, in *3D Cell Culture: Methods and Protocols*, ed. J. W. Haycock, Humana Press, Totowa, NJ, 2011, pp. 17–39, DOI: 10.1007/978-1-60761-984-0_2.
31 M. W. Tibbitt and K. S. Anseth, *Biotechnol. Bioeng.*, 2009, **103**, 655–663.
32 S. H. Lee and J. H. Sung, *Adv. Healthcare Mater.*, 2017, **7**, 1700419.
33 S. V. Murphy and A. Atala, *Nat. Biotechnol.*, 2014, **32**, 773–785.
34 D. P. N. Gonçalves, R. D. Rodriguez, T. Kurth, L. J. Bray, M. Binner, C. Jungnickel, F. N. Gür, S. W. Poser, T. L. Schmidt, D. R. T. Zahn, A. Androutsellis-Theotokis, M. Schlierf and C. Werner, *Acta Biomater.*, 2017, **58**, 12–25.
35 B. M. Crawford, R. L. Shammas, A. M. Fales, D. A. Brown, S. T. Hollenbeck, T. Vo-Dinh and G. R. Devi, *Int. J. Nanomed.*, 2017, **12**, 6259–6272.
36 L. Minai, D. Yeheskely-Hayon, L. Golan, G. Bisker, E. J. Dann and D. Yelin, *Small*, 2012, **8**, 1732–1739.
37 L. Minai, D. Yeheskely-Hayon and D. Yelin, *Sci. Rep.*, 2013, **3**, 2146.
38 L. Minai, A. Zeidan, D. Yeheskely-Hayon, S. Yudovich, I. Kviatkovsky and D. Yelin, *Nano Lett.*, 2016, **16**, 4601–4607.
39 B. S. Wiseman and Z. Werb, *Science*, 2002, **296**, 1046–1049.
40 Y. Mao, E. T. Keller, D. H. Garfield, K. Shen and J. Wang, *Cancer Metastasis Rev.*, 2013, **32**, 303–315.
41 T. G. Pestell, X. Jiao, M. Kumar, A. R. Peck, M. Prisco, S. Deng, Z. Li, A. Ertel, M. C. Casimiro, X. Ju, A. Di Rocco, G. Di Sante, S. Katiyar, A. Shupp, M. P. Lisanti, P. Jain, K. O. Wu, H. Rui, D. C. Hooper, Z. Yu, A. R. Goldman, D. W. Speicher, P. Laury-Kleintop and R. G. Lisa, *Oncotarget*, 2017, **8**, 81754–81775.
42 G. Brummer, D. S. Acevedo, Q. Hu, M. Portsche, W. Fang, M. Yao, B. Zinda, M. Myers, N. S. Alvarez, P. Fields, Y. Hong, F. Behbod and N. Cheng, *Mol. Cancer Res.*, 2017, **16**, 296–308.
43 V. P. Zharov, R. R. Letfullin and E. N. Galitovskaya, *J. Phys. D: Appl. Phys.*, 2005, **38**, 2571–2581.
44 H. Takahashi, T. Niidome, A. Nariai, Y. Niidome and S. Yamada, *Nanotechnology*, 2006, **17**, 4431.
45 V. Kotaidis, C. Dahmen, G. von Plessen, F. Springer and A. Plech, *J. Chem. Phys.*, 2006, **124**, 184702.
46 C. P. Lin and M. W. Kelly, *Appl. Phys. Lett.*, 1998, **72**, 2800–2802.
47 C. M. Pitsillides, E. K. Joe, X. Wei, R. R. Anderson and C. P. Lin, *Biophys. J.*, 2003, **84**, 4023–4032.
48 V. K. Pustovalov, A. S. Smetannikov and V. P. Zharov, *Laser Phys. Lett.*, 2008, **5**, 775.
49 F. Porta, G. Speranza, Ž. Krpetić, V. Dal Santo, P. Francescato and G. Scarì, *Mater. Sci. Eng., B*, 2007, **140**, 187–194.
50 A. Weiss, T. C. Preston, J. Popov, Q. Li, S. Wu, K. C. Chou, H. M. Burt, M. B. Bally and R. Signorell, *J. Phys. Chem. C*, 2009, **113**, 20252–20258.